Composites Part B 175 (2019) 107085

Contents lists available at ScienceDirect

Composites Part B

journal homepage: www.elsevier.com/locate/compositesb

# Recycled carbon fibre/$Bi_2Te_3$ and $Bi_2S_3$ hybrid composite doped with MWCNTs for thermoelectric applications

Priyanka Jagadish [a,b,**], Mohammad Khalid [a,*], Nowshad Amin [c,d], Mohammad Taghi Hajibeigy [e], Lau Phei Li [b], Arshid Numan [a,f], Nabisab Mujawar Mubarak [g], Rashmi Walvekar [e], Andy Chan [h]

[a] Graphene & Advanced 2D Materials Research Group (GAMRG), School of Science and Technology Sunway University, No. 5, Jalan Universiti, 47500, Bandar Sunway, Selangor, Malaysia
[b] Department of Chemical and Environmental Engineering, Faculty of Engineering, The University of Nottingham Malaysia Campus, 43500, Semenyih, Selangor, Malaysia
[c] Department of Electrical, Electronic and Systems Engineering, Faculty of Engineering and Built Environment, The National University of Malaysia, 43600, Bangi, Selangor, Malaysia
[d] Institute of Sustainable Energy, Universiti Tenaga Nasional, Jalan IKRAM-UNITEN, 43000, Kajang, Selangor, Malaysia
[e] Sustainable Energy and Green Technology Research Group, Faculty of Innovation and Technology, School of Engineering, Taylor's University Lakeside Campus, 47500, Subang Jaya, Selangor, Malaysia
[f] State Key Laboratory of ASIC and System, SIST, Fudan University, 200433, Shanghai, China
[g] Department of Chemical Engineering, Faculty of Engineering and Science, Curtin University, 98009, Sarawak, Malaysia
[h] Department of Civil Engineering, Faculty of Engineering, The University of Nottingham Malaysia Campus, 43500, Semenyih, Selangor, Malaysia

ARTICLE INFO

*Keywords:*
Bismuth telluride
Bismuth sulphide
Carbon nanotubes
Seebeck coefficient
Electrical resistivity
Thermoelectric

ABSTRACT

In this study, a cost-effective thermoelectric generator was developed from recycled carbon fibre (RCF) composites incorporated with multi-walled carbon nanotubes (MWCNT) doped bismuth telluride ($Bi_2Te_3$) and bismuth sulphide ($Bi_2S_3$). A facile approach utilising hot compression and brushing was used to prepare a cost-effective inorganic RCF thermoelectric composite with varying content of MWCNT ranging from 0.05 to 0.20 wt%. This work investigated the effect of doping MWCNT in $Bi_2Te_3$ and $Bi_2S_3$ matrix and its corresponding effect on thermoelectric, morphological, structural and thermal properties of RCF thermoelectric composite. The thermoelectric properties of RCF composites were optimised at 0.10 wt % (1.044 $\mu W K^{-2}m^{-1}$) and 0.15 wt% (0.849 $\mu W K^{-2}m^{-1}$) of MWCNT for doped $Bi_2Te_3$ and $Bi_2S_3$ respectively. The addition of MWCNT reduced the difference in power factor between RCF-$Bi_2Te_3$ and RCF-$Bi_2S_3$ from 52% to 19%. The presence of MWCNT in the $Bi_2S_3$ matrix overcame the high resistivity of $Bi_2S_3$ and improved its thermoelectric properties as MWCNT provided a conductive pathway for efficient electron transfer. Thus, MWCNT doped $Bi_2S_3$ RCF composites is an alternative to telluride free thermoelectric generators.

## 1. Introduction

Thermoelectric materials have received widespread attention over the past decade due to their rapidly emerging applications in waste heat energy harvesting. Thermoelectric materials/generators have the unique capability of directly converting waste heat to electricity by utilising the physical principle of Seebeck effect. Approximately 60–70% of waste heat is released into the environment during the combustion of fossil fuel-based energy resources, so the reuse of waste heat to electricity is plausible with thermoelectric materials/generators that are highly beneficial to energy savings [1,2].

Despite the numerous advantages offered by thermoelectric materials/generators, the commercialization of these materials, however, are limited by their high cost and low efficiency. Most industrially used thermoelectric generators are made from telluride based alloys (for low-temperature operation) and silicon germanium (for high-temperature operation) which require rare and expensive materials such as tellurium and germanium and therefore increasing the price of

* Corresponding author.
** Corresponding author. Graphene & Advanced 2D Materials Research Group (GAMRG), School of Science and Technology Sunway University, No. 5, Jalan Universiti, 47500, Bandar Sunway, Selangor, Malaysia.
*E-mail addresses:* priyankaj@sunway.edu.my (P. Jagadish), khalids@sunway.edu.my (M. Khalid).

https://doi.org/10.1016/j.compositesb.2019.107085
Received 1 November 2018; Received in revised form 9 June 2019; Accepted 1 July 2019
Available online 2 July 2019

thermoelectric generators [3]. These thermoelectric generators also have low thermal to electrical efficiency of less than 10% and a low figure of merit (ZT) values of less than unity [4,5]. One way to overcome the low efficiency and high cost of thermoelectric material is to search for low cost and highly efficient thermoelectric materials that could counteract the negative effect of low efficiency [6].

Though bismuth telluride ($Bi_2Te_3$) is a widely commercialised thermoelectric alloy, the scarcity and toxicity of tellurium have always been of pivotal concern [7]. Tellurium is one of the rarest stable solid element that only makes up 0.0000001% of the Earth's crust. Due to the poor availability of tellurium in the Earth's crust, it is vital that one look for alternatives to replace tellurium. A more environmentally friendly alternative is bismuth sulphide ($Bi_2S_3$), sulphur makes up 0.042% of the Earth's crust which makes sulphur 420,000 times more abundant than that of tellurium. With its low toxicity and natural abundance leading to lower cost, $Bi_2S_3$ is a good alternative to telluride based thermoelectric alloys.

In addition to its abundance, $Bi_2S_3$ has a band gap of 1.3 eV which is higher than that of $Bi_2Te_3$ at 0.17 eV which yields it to have naturally low carrier concentrations of $2 \times 10^{18}$ $cm^{-3}$ approximately two orders lower than $Bi_2Te_3$. $Bi_2S_3$ also has a higher Seebeck coefficient in the range of 150–480 μV/K [7,8] as compared to that of $Bi_2Te_3$ (60–250 μV/K) [9,10] owing to the difference in carrier concentration. In addition to that, $Bi_2S_3$ has a relatively lower thermal conductivity in the range of 0.4–0.85 W/mK [8] than that of $Bi_2Te_3$ (0.8–1.4 W/mK) [11], the higher Seebeck coefficient and lower thermal conductivity of $Bi_2S_3$ makes it a suitable replacement for telluride based alloys in thermoelectric applications. However, due to its intrinsically low carrier concentrations, it is mostly restricted by its poor electrical conductivity which could be resolved by extrinsic doping of $Bi_2S_3$ [7,12]. A few dopants such as bismuth (Bi) [8], bismuth chloride ($BiCl_3$) [12,13] and silver (Ag) [7] have been used in the past as electron dopants to tune the carrier concentration of $Bi_2S_3$ that successfully reduced the electrical resistivity of $Bi_2S_3$ and improved its corresponding power factor and ZT values.

In the recent past, multi-walled carbon nanotubes (MWCNT) have been investigated as an excellent platform for thermoelectric materials due to its nanoscale, low dimensional, holey structure features and its quantum confinement effect on charge carriers that is beneficial for improving power factor values [14].

Low dimensional nanostructures such as MWCNT are postulated to enhance the power factor of bulk thermoelectric materials through a mechanism called energy filtering [15]. In the presence of these nanostructures, low kinetic energy charge carriers are stopped by the energy barrier at nanostructure boundaries while high kinetic energy charge carriers are allowed to pass through them [16]. Concurrent improvement in Seebeck coefficient and electrical conductivity is plausible in the presence of this potential barrier eliminating low energy charge carriers and thereby improving charge carrier mobility [17].

Apart from using comparatively cheaper thermoelectric materials, further cost reduction of thermoelectric generators can be achieved by the utilization of recycled carbon fibre composites. Carbon fibre reinforced polymer (CFRP) composites are vastly utilised for automobile, aerospace and sports sectors due to its lightweight, low density and impressive mechanical properties. Due to its increased usage, there is a large amount of CFRP waste generated from manufacturing as well as at the end of life of the products [18,19]. However, incineration and landfilling are no longer viable options for disposal due to environmental and recycling regulations such as EU Directive on Landfill of Waste (Directive 99/31/EC) and End-of-life Vehicle Directive (Directive 2000/53/EC) [19]. Recycled carbon fibre (RCF) unfortunately cannot be reused for crucial mechanical and structural applications due to the declined mechanical properties after recycling. Thus, there is an imperative need to find an alternative for the reuse of RCF. Carbon fibres have exhibited positive thermoelectric capabilities in the past as films and composites owing to its electrical conductivity and weakly p-type thermoelectric nature [20–25].

$Bi_2S_3$-MWCNT hybrid composites have been employed in electronic devices such as lithium and sodium ion batteries [26–28], dye sensitised solar cells (DSSCs) [29] and pressure sensors [30] and has exhibited outstanding electrical performance. The inclusion of MWCNT in $Bi_2S_3$ can serve as a conducting pathway promoting efficient transportation of electron thereby enhancing its electrical properties [31]. Although $Bi_2S_3$-MWCNT hybrid composites were used in energy storage, sensor and solar applications, to the best of author's knowledge, there are no studies reported in the literature thus far on the thermoelectric properties of $Bi_2S_3$-MWCNT hybrid composites.

Most of the research work pertaining MWCNT-$Bi_2Te_3$ composite was fabricated via ball milling/mechanical alloying complemented with spark plasma sintering reported an increase in the electrical resistivity of $Bi_2Te_3$ alloy upon the incorporation of MWCNT [32,33]. This increase in resistivity is may be due to the defects introduced on carbon nanotubes during the milling process that may have altered its conductive networks [34]. In this study, MWCNTs will be incorporated in the $Bi_2Te_3$ matrix as a hybrid composite without inducing surface defects on the carbon nanotubes and its resulting electrical properties will be investigated.

As a continuation of our previous work [22], this work focuses on fabricating a cost-effective thermoelectric generator by incorporating MWCNT doped $Bi_2Te_3$ and $Bi_2S_3$ onto recycled carbon fibre composites to further improve the electrical conductivity and the subsequent thermoelectric properties of RCF composites. This study investigated the effect of varying concentrations of MWCNT on the thermoelectric, morphology, structural and thermal stability properties of both RCF-$Bi_2Te_3$ and RCF-$Bi_2S_3$ composites.

## 2. Experimental

### 2.1. Materials

Commercial bismuth (III) telluride (purity: 99.99%) and bismuth (III) sulphide (purity: 99.99%) with a relative density of 7.6 g/$cm^3$ and 7.7 g/$cm^3$ respectively were obtained from Sigma Aldrich Sdn. Bhd to be used as inorganic thermoelectric fillers. Acrodur DS 3530, a water-based and formaldehyde free binding polymer was supplied by BASF Malaysia Sdn. Bhd. Recycled Toray T600 carbon fibres which were recovered from a fluidised bed process was supplied by Recycled Carbon Fibre Limited (RCF) Coseley, UK. Ethylene glycol from R&M Chemicals and MWCNTs with outer diameter 20–30 nm, length of ~30 μm and purity of 95 wt% were supplied by Chengdu Organic Chemicals Co. Ltd.

### 2.2. Fabrication of RCF thermoelectric composite

#### 2.2.1. Fabrication of bare RCF composite

The methodology in this section has been adapted from the author's previous work [22]. Randomly oriented RCF sheets were soaked for 15 min in a solution consisting of Acrodur DS 3530 binder and water with a volume ratio of 1: 10 parts. After soaking, the RCF was placed between two metal plates lined with laboratory wipes to eliminate excess water. A brick load of 10 kg was then placed on the sandwiched RCF to obtain a uniform composite with a thickness of 1 mm. The same steps were repeated three times until RCF was completely free from residual water. The dried RCF was then subjected to an applied load of 5 kg was and placed in a gravity convection oven (UN 55, Memmert) at 200 °C for 1 h for the curing and formation of bare RCF composite.

#### 2.2.2. MWCNT doped thermoelectric filler coating on RCF composite

The MWCNTs were suspended in ethylene glycol and subjected to ultrasonication for 1 h. Then, the thermoelectric filler particles ($Bi_2Te_3$ and $Bi_2S_3$) and Acrodur 3530 binder was added to the ultrasonicated MWCNT suspension and is subjected again for another 1 h of ultrasonication. The MWCNT doped thermoelectric filler coating was paint brushed on to the surface of bare RCF composite and placed into the

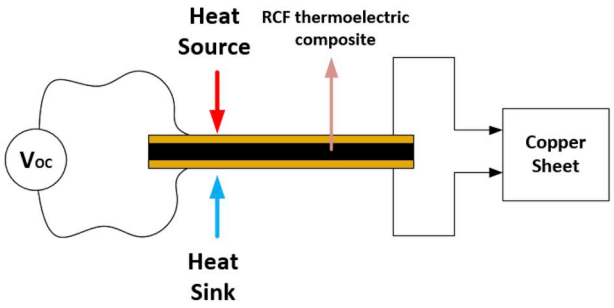


**Fig. 1.** Schematic set up for Seebeck coefficient measurement of RCF thermoelectric composite.

oven at 200 °C for 1 h. The concentration of MWCNT was varied from 0.05 to 0.20 wt%.

### 2.3. Thermoelectric properties measurement

#### 2.3.1. Measurement of seebeck coefficient

The measurement of Seebeck coefficient in this study was carried out using an in-house fabricated measurement system as shown in Fig. 1.

The formula in Eq (1) was used to compute the Seebeck coefficient:

$$\alpha = \frac{\Delta V}{\Delta T} = \frac{V_H - V_C}{T_H - T_C} \quad (1)$$

Where the potential difference created between the hot side, $V_H$ and cold side, $V_C$ is measured in millivolts as ΔV. The temperature difference produced between the temperature on the hot side, $T_H$ and temperature on the cold side, $T_c$ is represented as ΔT. Seebeck coefficient measurement was carried out with a hot side temperature of approximately 40 °C and the cold side was placed at room temperature.

An average of six readings was taken to compute the Seebeck coefficients of the RCF thermoelectric composites using Eq (1).

### 2.4. Measurement of electrical resistivity

HMS ECOPIA 3000 with a magnetic field 0.57 T and probe current of 15 mA was used to measure the electrical resistivity, carrier concentration and carrier mobility of the RCF thermoelectric composites.

### 2.5. Power factor calculation

Power factor (PF) was used to measure the efficiency of the thermoelectric composite using Eq (2) [35].

$$PF = \frac{\alpha^2}{\rho} \quad (2)$$

The measured values of both Seebeck coefficient, $\alpha$ and electrical resistivity, $\rho$ was used to compute the PF.

### 2.6. Characterisation

#### 2.6.1. Thermogravimetric analysis (TGA)

Thermogravimetric analyser (Perkin Elmer STA 6000) was used to study the thermal degradation and stability of the composites. The samples are subjected to an air flow rate of 20 mL/min and heated from 30 °C to 900 °C with a heating rate of 10 °C/min. The temperature at 5% weight loss is denoted as the onset degradation temperature ($T_{onset}$). The temperature at which the RCF thermoelectric composites experiences maximum weight loss is denoted as maximum degradation temperature ($T_{max}$). $T_{onset}$ and $T_{max}$ were used to show the thermal degradation and stability of the RCF thermoelectric composites.

### 2.7. X-ray powder diffraction

X-ray powder diffraction (XRD) (Cu-Kα, Bruker D8 Advance) operating at 40 kV and 40 mA was used to identify the phase structure and crystallinity property. Cu Kα radiation wavelength of 1.540 Å with a step size of 0.025 was used to obtain the XRD patterns in the 2$\theta$ range from 10 to 80°.

Scherrer equation as depicted in Eq (3) was used to compute crystallite size (D) [36]:

$$D = \frac{0.9\lambda}{\beta cos\theta} \quad (3)$$

Where $\lambda$ is the wavelength of x-ray (1.540 Å), $\theta$ is the Bragg diffraction angle, $\beta$ is the full width at half maximum (FWHM) of the dominant peak.

Eq (4) was utilised to calculate the microstrain ($\varepsilon$) of the RCF thermoelectric composites [37]:

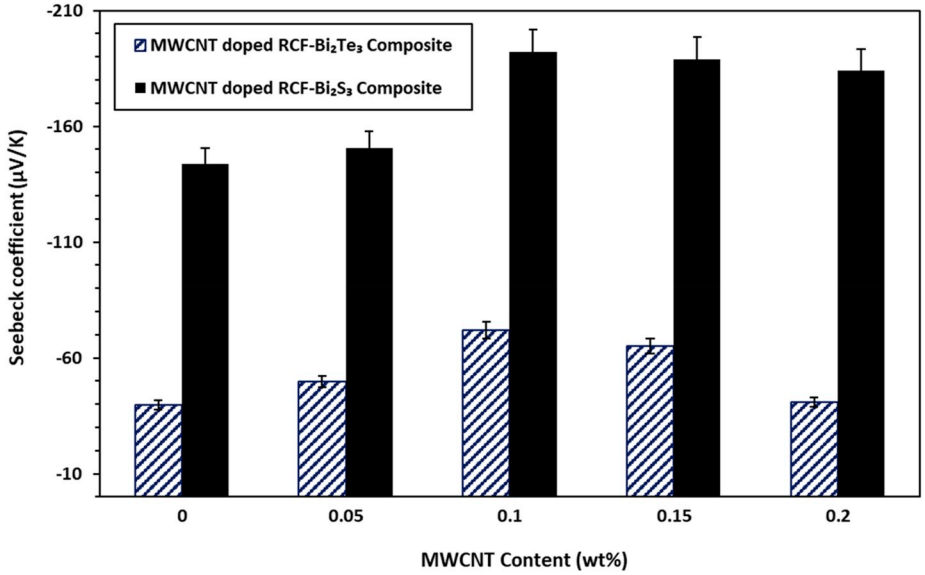


**Fig. 2.** Seebeck coefficient of RCF-$Bi_2Te_3$ and RCF-$Bi_2S_3$ composites doped with varying amounts of MWCNT.

**Table 1**
The effect of doping RCF-$Bi_2Te_3$ and RCF-$Bi_2S_3$ composites with varying MWCNT concentrations on the carrier concentration and carrier mobility.

| MWCNT content (wt%) | Carrier concentration of MWCNT doped RCF-$Bi_2Te_3$ composites ($cm^{-3}$) | Carrier mobility of MWCNT doped RCF-$Bi_2Te_3$ composites ($cm^2V^{-1}s^{-1}$) | Carrier concentration of MWCNT doped RCF-$Bi_2S_3$ composites ($cm^{-3}$) | Carrier mobility of MWCNT doped RCF-$Bi_2S_3$ composites ($cm^2V^{-1}s^{-1}$) |
|---|---|---|---|---|
| 0.00 | $6.01 \times 10^{20}$ | $1.27 \times 10^{-2}$ | $4.27 \times 10^{18}$ | $6.67 \times 10^{-2}$ |
| 0.05 | $0.83 \times 10^{20}$ | $10.30 \times 10^{-2}$ | $4.07 \times 10^{18}$ | $22.7 \times 10^{-2}$ |
| 0.10 | $0.96 \times 10^{20}$ | $13.20 \times 10^{-2}$ | $0.541 \times 10^{18}$ | $248 \times 10^{-2}$ |
| 0.15 | $1.29 \times 10^{20}$ | $11.30 \times 10^{-2}$ | $0.543 \times 10^{18}$ | $273 \times 10^{-2}$ |
| 0.20 | $2.10 \times 10^{20}$ | $6.75 \times 10^{-2}$ | $0.590 \times 10^{18}$ | $252 \times 10^{-2}$ |

$$\varepsilon = \frac{\beta}{4 \tan \theta} \tag{4}$$

Dislocation density ($\delta$) within the composites was calculated using Eq (5) [38]:

$$\delta = \frac{1}{D^2} \tag{5}$$

#### 2.7.1. Field emission scanning electron microscope (FESEM)

The surface morphology of the RCF thermoelectric composites was obtained using FEI Quanta 400F.

## 3. Results and discussion

### 3.1. Effect of MWCNT on the thermoelectric properties of RCF-$Bi_2Te_3$ and RCF-$Bi_2S_3$

The effect of varying the concentration of MWCNT on the Seebeck coefficient, electrical resistivity, and the power factor of RCF-$Bi_2Te_3$ and RCF-$Bi_2S_3$ composites respectively are shown in Fig. 2 to Fig. 4. In Fig. 2, there is a noteworthy improvement in the Seebeck coefficient of RCF-$Bi_2Te_3$ and RCF-$Bi_2S_3$ composites upon the incorporation of MWCNTs at certain optimum concentrations. The introduction of nanostructures such as MWCNTs at appropriate concentrations into bulk materials such as $Bi_2Te_3$ and $Bi_2S_3$ are known to introduce interfaces within the thermoelectric matrix [39]. The incorporation of MWCNTs within the RCF-$Bi_2Te_3$ and RCF-$Bi_2S_3$ composites introduced two interfaces: (a) MWCNT/($Bi_2Te_3$ or $Bi_2S_3$ interface) and (b) MWCNT/insulating polymer. These interfaces are thought to induce an energy filtering effect that forms potential boundaries that are capable of filtering out lower energy carriers while higher energy carriers are allowed to pass through them thus increasing the mean energy of carriers in the path [15,39]. Seebeck coefficient of both RCF-$Bi_2Te_3$ and RCF-$Bi_2S_3$ composites was highest at 0.10 wt% of MWCNT and their Seebeck coefficients improved by approximately 80% and 34% respectively compared to its non-doped counterpart (0 wt% of MWCNT) due to the above mentioned filtering effect.

Doping with MWCNTs at a certain optimum concentration resulted in decreased carrier concentrations as shown in Table 1, thus leading to increased Seebeck coefficient of both RCF-$Bi_2Te_3$ and RCF-$Bi_2S_3$ composites. The optimum loading of MWCNTs for RCF-$Bi_2Te_3$ and RCF-$Bi_2S_3$ composites was 0.10 wt% and 0.15 wt% respectively, at these optimum loadings carrier concentrations decreased (by 84% and 87% respectively) and carrier mobility improved (by 939% and 3992%) as shown in Table 1 due to the energy filtering mechanism. This decreased carrier concentration is a validation of the energy filtering effect mechanism occurring within the composite by removing low energy carriers with the incorporation of MWCNTs. The improvement of charge transport within the inorganic matrix ($Bi_2Te_3$ and $Bi_2S_3$) and a non-conducting polymer matrix (polymeric binder) also led to higher Seebeck coefficients due to high levels of carrier mobility in MWCNTs [40,41].

However, at higher concentrations of MWCNTs (0.15 wt% and 0.20 wt%) (as shown in Fig. 2) there was a gradual decrease in its Seebeck coefficient for both RCF-$Bi_2Te_3$ and RCF-$Bi_2S_3$ with the subsequent increase in carrier concentrations as shown in Table 1. As MWCNTs are p-type with Seebeck coefficients normally in the range of +40–50 μV/K [42], the drop in Seebeck coefficient at higher concentrations of MWCNTs may be due to the dominating p-type doping effect over the n-type $Bi_2Te_3$/$Bi_2S_3$ particles [43]. At higher concentrations, MWCNT prevented $Bi_2Te_3$/$Bi_2S_3$ particles from connecting with each other as shown in Fig. 7 (c), Figs. 7 (d) and Fig. 8 (d) owing to the agglomeration of MWCNT and does not disperse well in the $Bi_2Te_3$/$Bi_2S_3$ matrix, thus playing the role of an impurity. A similar doping effect that decreased Seebeck coefficient of $Bi_2Te_3$ at higher concentration of carbon nanotubes was also observed and reported by Bark et al. [43] using MWCNT, Zhang et al. [41] using single wall carbon nanotubes (SWCNTs) and Lognone and Gascoin [34] using MWCNTs on n-type $Bi_2Te_{2.4}Se_{0.6}$.

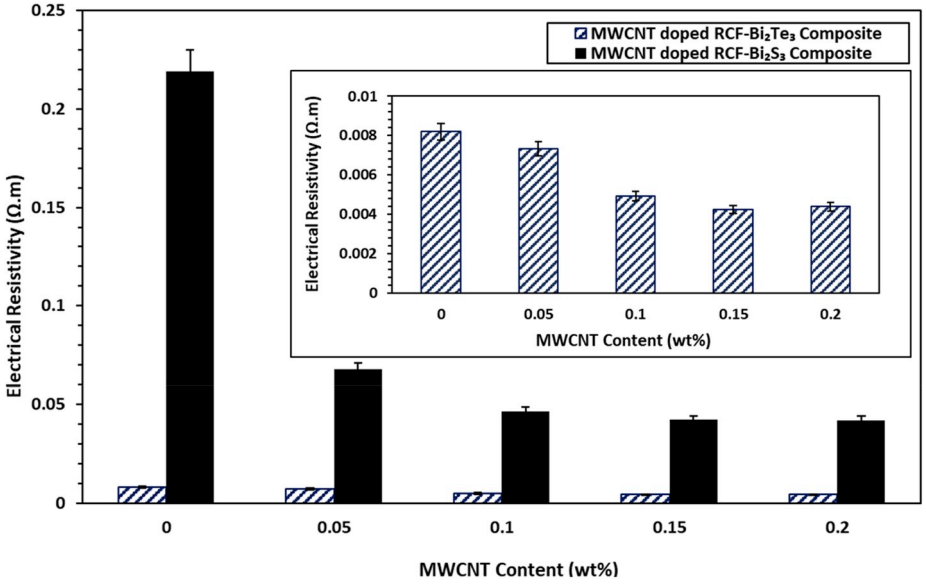


**Fig. 3.** Electrical resistivity of RCF-$Bi_2Te_3$ and RCF-$Bi_2S_3$ composites doped with varying amounts of MWCNT (inset: zoomed view of electrical resistivity of RCF-$Bi_2Te_3$ composites with varying amounts of MWCNT).

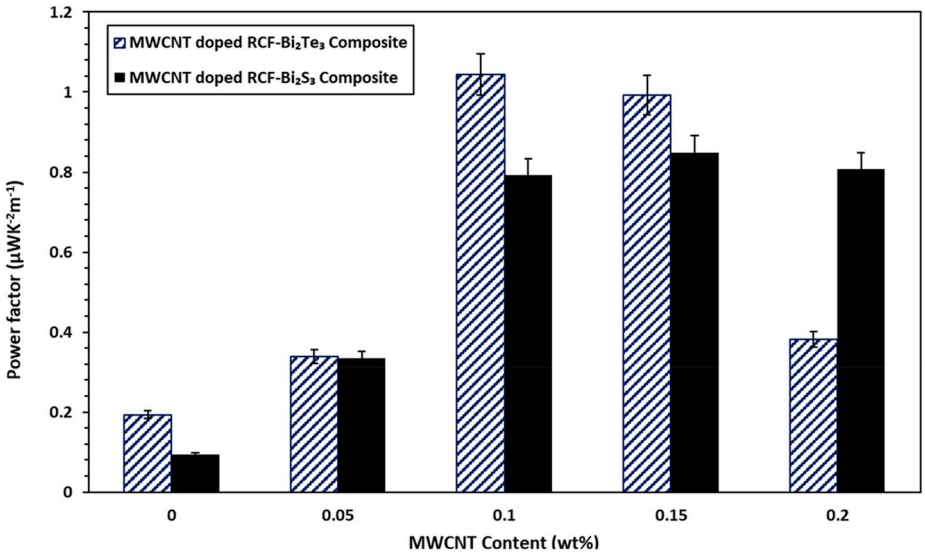


**Fig. 4.** Power factor of RCF-$Bi_2Te_3$ and RCF-$Bi_2S_3$ composites doped with varying amounts of MWCNT.

Carrier concentration also exhibit an increasing trend at 0.15 and 0.20 wt% as shown in Table 1, this is because the energy filtering mechanism is no longer viable at higher concentrations of MWCNT as the MWCNTs are agglomerated and do not form interfaces with the $Bi_2Te_3$/$Bi_2S_3$ particles, thus allowing higher amount of charge carriers to pass through with lower energy (i.e carrier mobility) which ultimately decreases Seebeck coefficient of RCF-$Bi_2Te_3$ and RCF-$Bi_2S_3$ composites. The energy filtering effect in most cases is only observed to be present at intermediate doping levels when the dopant is filling in interstitial spaces between $Bi_2Te_3$/$Bi_2S_3$ particles and insulating polymer [15,44].

As illustrated in Fig. 3, increasing concentrations of MWCNTs decreased the electrical resistivity of RCF-$Bi_2Te_3$ composites. This is because of the massive improvement in carrier mobility as depicted in Table 1 (939% improvement at 0.10 wt% of MWCNT) that was brought about by the presence of MWCNTs in the RCF-$Bi_2Te_3$ composites. The continuous decrease of resistivity with an increasing amount of MWCNTs is because MWCNTs formed conducting channels to transport electrons between $Bi_2Te_3$ particles and the insulating polymer [45,46]. A reducing trend of electrical resistivity was noted from 0.05 to 0.15 wt % of MWCNT, the resistivity of the RCF-$Bi_2Te_3$ composite was reduced by approximately 40% at 0.10 wt% of MWCNT. Other research works that incorporated MWCNT into $Bi_2Te_3$ alloy using ultrasonic [41,47], hydrothermal [33] and electrodeposition [48,49] also reported a decrease in the electrical resistivity of $Bi_2Te_3$ alloy composites similar to that observed in this study. However, at 0.20 wt% of MWCNT for RCF-$Bi_2Te_3$ composites, a slight increase in resistivity is observed however still more conductive than that of 0 wt% MWCNT is observed as it is plausible that at larger concentrations MWCNT may play the role of impurities that prevent $Bi_2Te_3$ particles from connecting with each other resulting in decreased carrier mobility [43].

As depicted in Fig. 3, the electrical resistivity of RCF-$Bi_2S_3$ composites is also seen to decrease upon the incorporation of MWCNTs at all concentrations, however, at higher loadings of 0.15 wt% and 0.20 wt% of MWCNT, the resistivity remained constant. The substantial improvement in carrier mobility at 0.15 wt% of MWCNT (by approximately 3992%) has helped to reduce the electrical resistivity of RCF-$Bi_2S_3$ composites by approximately 81% when compared to 0 wt% of MWCNT. Although there was an 87% decrease in carrier concentration for RCF-$Bi_2S_3$ composites as shown in Table 1, the staggering improvement of 3992% in carrier mobility helped to decrease the electrical resistivity by 81%. A similar decrease in resistivity with increasing concentration of MWCNTs was also observed by Yu et al. (2008) and Moriarty et al. (2012) that doped a non-conducting polymer poly (vinyl acetate) (PVAc) with CNT [42,44]. Both, the cited studies mentioned that significant enhancement in electrical conductivity is plausible with MWCNT fillers as MWCNT forms conductive networks through the insulating polymer.

The power factor as shown in Fig. 4, is one of the most important factors that monitors thermoelectric properties. The power factor of RCF-$Bi_2Te_3$ composites increased by a staggering 75–440% upon the varying incorporation of MWCNTs. The power factor was observed to increase from 0 wt% to 0.10 wt% of MWCNT, and then gradually dropped from 0.15 wt% to 0.20 wt% of MWCNT. The improvement in power factor was greatly contributed by enhanced electrical conductivity and Seebeck coefficient upon the incorporation of MWCNT from 0.05 wt% to 0.15 wt% of MWCNT. The improved power factor is stemming from the energy filtering effect at MWCNT/$Bi_2Te_3$ and also MWCNT/insulating polymer interfaces which formed potential barriers that allow only carriers with energy to pass, thus increasing the mean carrier energy in the flow. This proposed phenomenon is supported by the drastic decrease in carrier concentration while the carrier mobility increased exponentially as shown in Table 1. A similar observation was made by Du et al. [47] in which a concurrent enhancement in the Seebeck coefficient and electrical conductivity was reported due to the inclusion of graphene that induced the energy filtering effect.

The power factors of RCF-$Bi_2S_3$ composites doped with MWCNTs are also shown in Fig. 4. The power factors of RCF-$Bi_2S_3$ composites improved by approximately 800% upon the incorporation of 0.15 wt% of MWCNT due to the simultaneous improvement in electrical conductivity and Seebeck coefficient. The power factor showed significant improvement from 0.05 to 0.10 wt% MWCNT, however, from 0.15 to 0.20 wt% MWCNT there was minimal improvement. This indicates that at lower doping concentrations MWCNT can effectively enhance carrier transportation owing to the energy filtering mechanism. However, at higher concentrations (0.20 wt%) of MWCNT, an opposite effect is observed, whereby the MWCNT acts as a degenerate (highly doped) semiconductor that exhibits a metallic behaviour. Thus, increasing its carrier concentration and leading to decreased Seebeck coefficient. Thus, the optimum doping level of MWCNT for RCF-$Bi_2Te_3$ and RCF-$Bi_2S_3$ is 0.10 wt% and 0.15 wt% of MWCNTs with a power factor of 1.044 and 0.849 $\mu W\,K^{-2}m^{-1}$ respectively.

### 3.2. *Morphological study of RCF-$Bi_2Te_3$ and RCF-$Bi_2S_3$ composites doped with MWCNT*

Fig. 5 shows the FESEM images of RCF-$Bi_2Te_3$ and RCF-$Bi_2Te_3$ doped

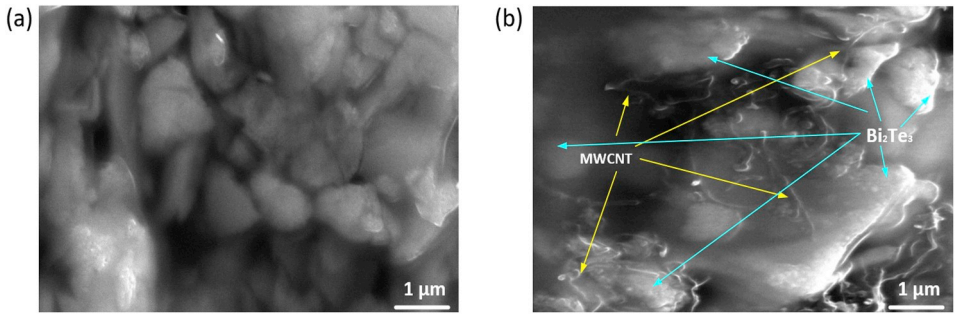


**Fig. 5.** FESEM images of (a) RCF-$Bi_2Te_3$ composite (b) RCF-$Bi_2Te_3$ doped with 0.05 wt% of MWCNT.

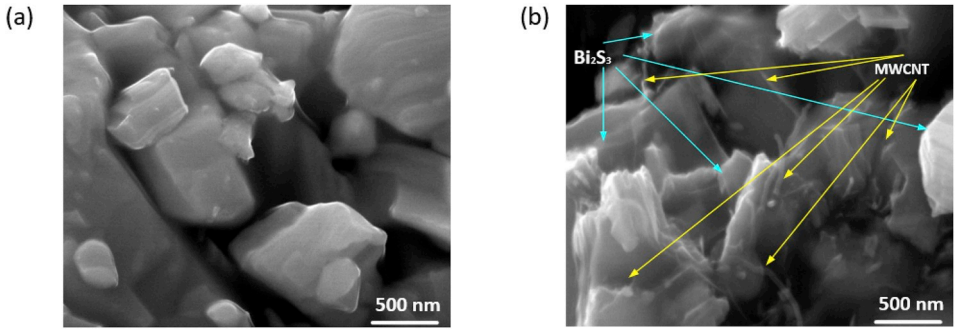


**Fig. 6.** FESEM images of (a) RCF-$Bi_2S_3$ composite (b) RCF-$Bi_2S_3$ doped with 0.05 wt% of MWCNT.

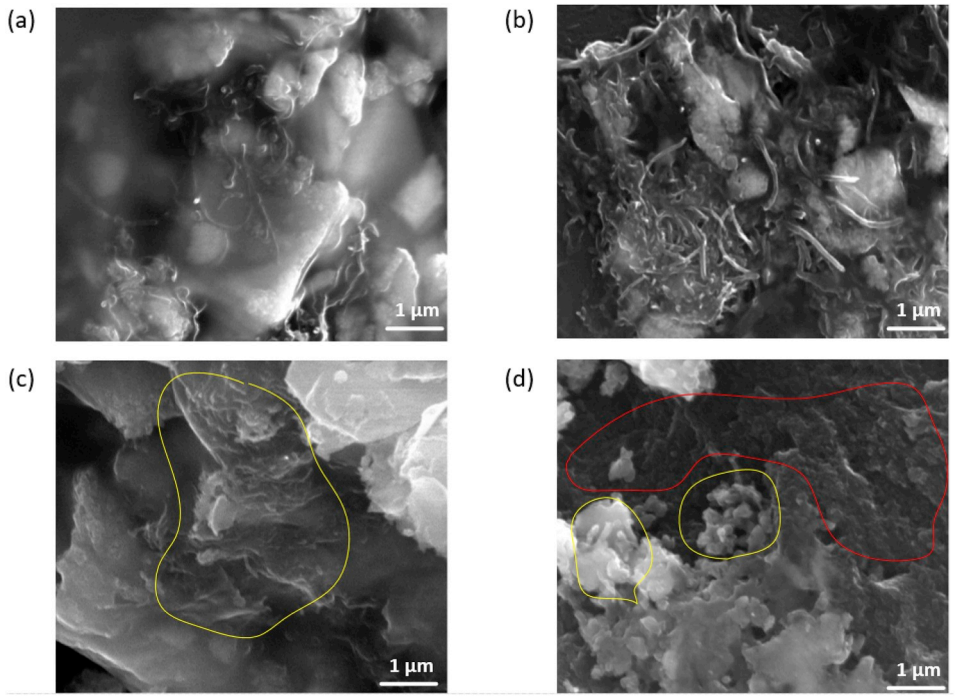


**Fig. 7.** FESEM images of RCF-$Bi_2Te_3$ composites doped with (a) 0.05 wt% of MWCNT (b) 0.10 wt% of MWCNT (c) 0.15 wt% of MWCNT (d) 0.20 wt% of MWCNT.

with MWCNT composite. The granular structures are shown in Fig. 5 (b) (as indicated by the blue arrows) are referring to the $Bi_2Te_3$ particles while the worm-like structures (as indicated by the yellow arrows) are referring to the MWCNTs. The MWCNTs are well dispersed in the polymer-$Bi_2Te_3$ matrix and filled the inter-spaces between $Bi_2Te_3$ particles leading to the formation of a conductive pathway within the matrix. Similar morphology was also observed in the RCF-$Bi_2S_3$ composites doped with MWCNT as shown in Fig. 6 (b). A higher magnification was used to study the interaction of MWCNT within the RCF-$Bi_2S_3$ composite as this was the lowest magnification that could clearly visualise the interaction. The MWCNTs is also seen to form a conductive pathway between the $Bi_2S_3$ particles within the insulating polymer matrix. The 81% reduction in electrical resistivity of MWCNT doped RCF-$Bi_2S_3$ composites mentioned in Section 3.1 is due to the presence of this conductive network.

The morphology of RCF-$Bi_2Te_3$ composites with increasing

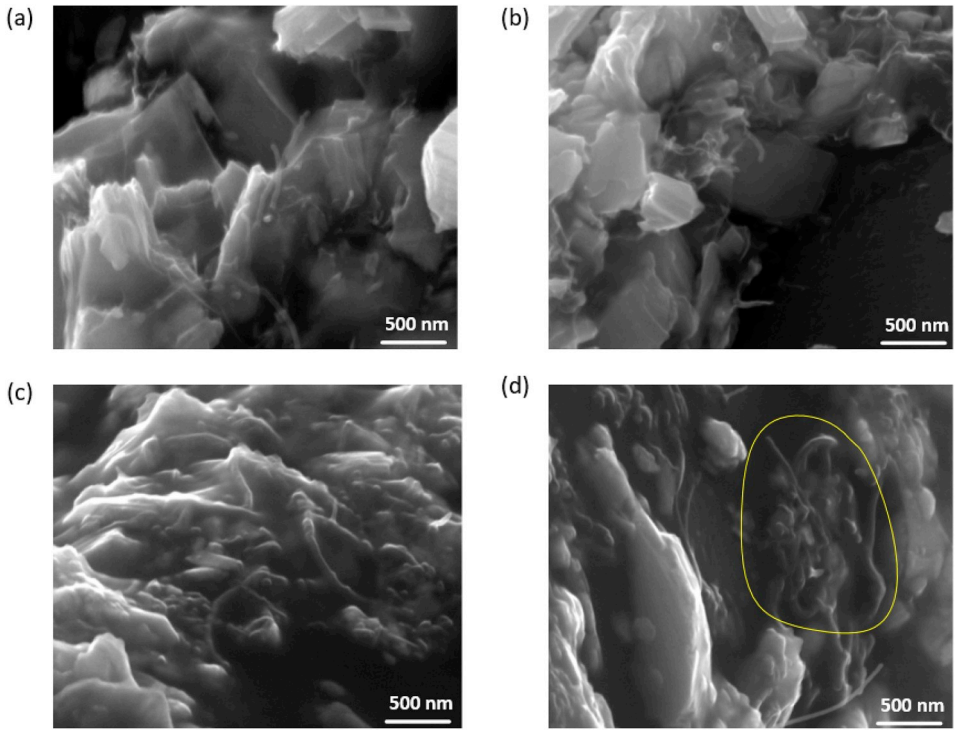


**Fig. 8.** FESEM images of RCF-$Bi_2S_3$ composites doped with (a) 0.05 wt% of MWCNT (b) 0.10 wt% of MWCNT (c) 0.15 wt% of MWCNT (d) 0.20 wt% of MWCNT.

concentrations of MWCNTs is shown in Fig. 7. The MWCNTs are seen to be well dispersed within the polymer-$Bi_2Te_3$ matrix at 0.05 and 0.10 wt % of MWCNT, however, at 0.15 and 0.20 wt% it can be seen that MWCNTs are beginning to concentrate in a particular portion of the $Bi_2Te_3$ polymer matrix owing to the length of the carbon nanotubes as highlighted by the yellow circle in Fig. 7 (c) and Fig. 7 (d). These higher concentrations of MWCNTs may have possibly hindered carrier mobility leading to decreased carrier mobility as shown in Table 1, thus leading to lower Seebeck coefficient at 0.15 and 0.20 wt% than that at 0.10 wt% of MWCNT. At 0.20 wt% of MWCNT as shown in Fig. 7 (d), agglomerates of MWCNT (as highlighted by the yellow circle) is formed and there is also a separation of the granular structures of $Bi_2Te_3$ and the worm-like structures of MWCNTs (as highlighted by the red circle). These agglomeration and separation could be the reason for the increased electrical resistivity at 0.20 wt% of MWCNT.

For the RCF-$Bi_2S_3$ composites doped with MWCNT as shown in Fig. 8,

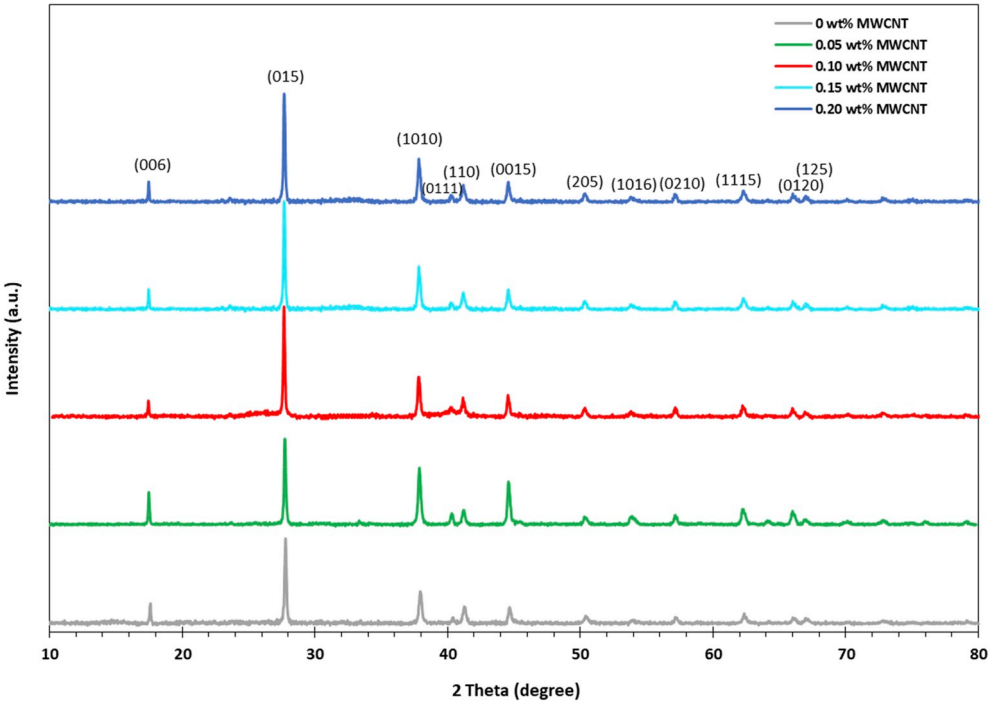


**Fig. 9.** XRD pattern of MWCNT doped RCF-$Bi_2Te_3$ composites.

**Table 2**
The effect of doping RCF-$Bi_2Te_3$ composites with varying MWCNT concentrations on the dislocation density, microstrain, crystallite size and FWHM.

| MWCNT Concentrations (wt %) | FWHM (radian) | Crystallite size, D (nm) | Microstrain ($\varepsilon$ x $10^{-3}$) (lines$^{-2}$ m$^{-4}$) | Dislocation density ($\delta$ x $10^{14}$) (lines/m$^2$) |
|---|---|---|---|---|
| 0.00 | 0.0030 | 47.01 | 3.1 | 4.52 |
| 0.05 | 0.0028 | 51.12 | 2.8 | 3.83 |
| 0.10 | 0.0026 | 55.26 | 2.6 | 3.27 |
| 0.15 | 0.0025 | 57.60 | 2.5 | 3.01 |
| 0.20 | 0.0025 | 57.20 | 2.5 | 3.06 |

the MWCNT is seen to be well dispersed at all doping concentrations within the $Bi_2S_3$-polymeric matrix. Though no agglomerates of MWCNT was observed in the case of RCF-$Bi_2S_3$ composites, a small well of concentrated MWCNT (as highlighted by the yellow circle) in Fig. 8 (d) was observed within the matrix at 0.20 wt%, which may have contributed to reduced mobility as shown in Table 1. At higher concentrations of MWCNTs, it is observed that the power factors of both RCF-$Bi_2Te_3$ and RCF-$Bi_2S_3$ composites decreased, this could be due to the decreased interfaces between that of MWCNT and the thermoelectric particles, as shown in the FESEM images that is responsible for the energy filtering mechanism.

### *3.3. The effect of MWCNT doping on the XRD of RCF-$Bi_2Te_3$ and RCF-$Bi_2S_3$ composites*

XRD patterns of RCF-$Bi_2Te_3$ and RCF-$Bi_2Te_3$ doped with MWCNT composites are shown in Fig. 9. In general, the obtained XRD patterns of all samples were similar to that of $Bi_2Te_3$. No visible peak corresponding to MWCNT in RCF-$Bi_2Te_3$ doped MWCNT composites was observed due to the low amount of MWCNT in the composites. A lack of MWCNT peak in XRD was also observed in several other $Bi_2Te_3$-MWCNT hybrid composite studies owing to its low doping amount [39,41,43,48]. The most prominent peak in the case of all XRD patterns is (015) which were used to calculate all XRD related parameters such as FWHM, crystallite size, dislocation density and microstrain. The D, $\varepsilon$ and $\delta$ of the RCF-$Bi_2Te_3$ and MWCNT doped RCF-$Bi_2Te_3$ composites are as shown in Table 2.

The intensity of XRD patterns increased with increasing concentrations of MWCNT as shown in Fig. 9, showing that incorporation of MWCNT enhanced the crystallinity of RCF-$Bi_2Te_3$ composite. The addition of MWCNT helps reduce the amorphous nature of the insulating polymer used in this study. The improvement in crystallinity is also complemented by the decrease in the FWHM values as shown in Table 2 upon the incorporation of MWCNT. The improvement in crystallinity was also noted by Refs. [48,49] upon the incorporation of MWCNTs.

The crystallite size, D also increased with the incorporation of MWCNT, however, remained almost constant after 0.15 wt%. The increase in crystallite size could be attributed to MWCNTs attaching itself to the $Bi_2Te_3$ particles as the conductive networks are formed throughout the matrix as shown in Fig. 7. The microstrain and dislocation density as shown in Table 2 are also seen to decrease until 0.15 wt% of MWCNT, these structural properties also reflected in decreased electrical resistivity of the RCF-$Bi_2Te_3$ composites with MWCNTs as shown in Fig. 3. However, as agglomerates of MWCNTs are formed at 0.20 wt% it resulted in increased dislocation density and electrical resistivity followed by the decreased power factor.

XRD patterns of RCF-$Bi_2S_3$ and RCF-$Bi_2S_3$ doped with MWCNT composites are shown in Fig. 10. All XRD patterns shown in Fig. 10 have the following 27 diffraction peaks of $Bi_2S_3$ was observed on all the RCF-$Bi_2S_3$ composite were located at 2θ, 15.75°, 17.62°, 22.43°,24.99°, 25.23°, 27.49°, 28.65°, 31.84°, 33.04°, 33.96°, 35.65°, 36.68°, 39.09°, 39.95°, 45.60°, 46.51°, 47.05°, 48.48°, 49.21°, 52.63°, 53.86°, 54.77°, 62.68°, 64.57°, 72.04°,73.05° and 76.21° corrsoponding to the (200), (201), (202), (301), (103), (210), (112), (212), (013), (303), (402), (312), (410), (411), (020), (314), (511), (600), (512), (321), (610), (611), (711), (712), (606), (417) and (408) lattice planes, respectively. Similar to that of RCF-$Bi_2Te_3$ composites, the obtained XRD patterns of all samples were similar to that of $Bi_2S_3$. No visible peak corresponding to MWCNT in RCF-$Bi_2S_3$ doped MWCNT composites was observed due to the low amount of MWCNT in the composites. A lack of MWCNT peak in XRD was also observed in several other $Bi_2S_3$-MWCNT hybrid composite studies owing to its low doping amount [27,28]. The most dominant peak in case of all XRD patterns is (301) was used for the calculation of XRD parameters.

Similar to that of MWCNT doped RCF-$Bi_2Te_3$, RCF-$Bi_2S_3$ also exhibited a decreasing pattern of the FWHM values, upon the incorporation of MWCNTs which denotes an improvement in the crystallinity as shown in Table 3. It can be seen that crystallite size, D also increased from 52.14 nm to a maximum value of 57.69 nm with increasing

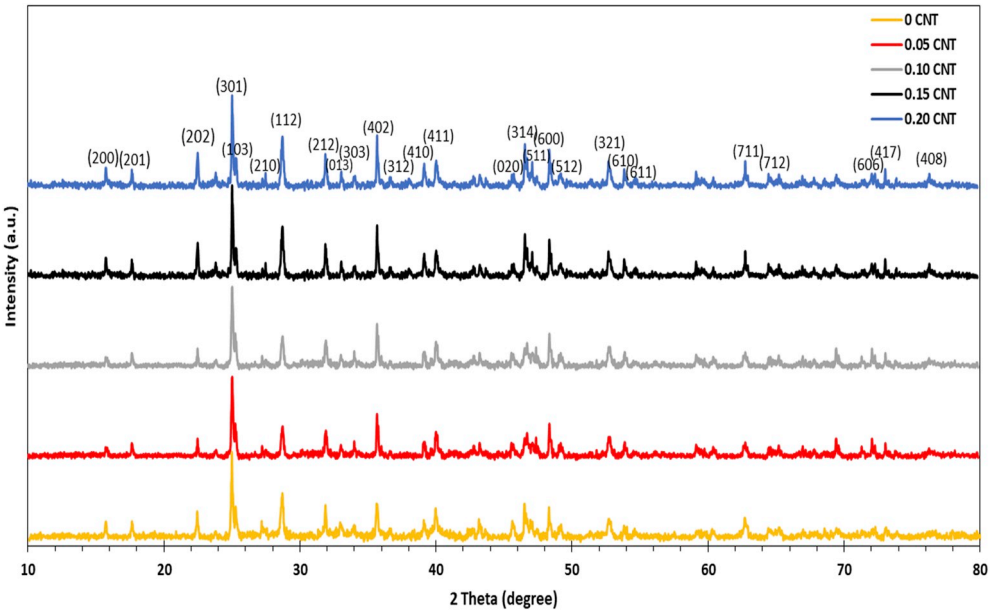


**Fig. 10.** XRD pattern of MWCNT doped RCF-$Bi_2S_3$ composites.

**Table 3**
The effect of doping RCF-$Bi_2S_3$ composites with varying MWCNT concentrations on the dislocation density, microstrain, crystallite size and FWHM.

| MWCNT Concentrations (wt %) | FWHM (radian) | Crystallite size, D (nm) | Microstrain ($\varepsilon$ x $10^{-3}$) (lines$^{-2}$ m$^{-4}$) | Dislocation density ($\delta$ x $10^{14}$) (lines/m$^2$) |
|---|---|---|---|---|
| 0.00 | 0.00272 | 52.14 | 3.1 | 3.68 |
| 0.05 | 0.00267 | 53.16 | 3.0 | 3.54 |
| 0.10 | 0.00261 | 54.23 | 2.9 | 3.40 |
| 0.15 | 0.00248 | 57.28 | 2.8 | 3.05 |
| 0.20 | 0.00246 | 57.69 | 2.8 | 3.00 |

concentration of MWCNT. This may be due to the conductive network of MWCNT that is attaching itself to the crystals of $Bi_2S_3$ particles as shown in Fig. 8. However, at higher concentrations of MWCNTs (0.20 wt%), there is no observable change in D perhaps because the interaction between $Bi_2S_3$ particles and MWCNTs are lower with an observable concentration/accumulation of MWCNTs in the polymer phase at 0.20 wt% with not much connection to that of $Bi_2S_3$ particles as shown in Fig. 8 (d).

With the increase in D, the decrease in microstrain, $\varepsilon$ and dislocation density, $\delta$ are widely known phenomenon [50]. The continuous decrease in both $\varepsilon$ and $\delta$ resulted in an 81% decrease in electrical resistivity for 0.15 wt% MWCNT doped RCF-$Bi_2S_3$ composites as compared to that of 0 wt% MWCNT as shown in Fig. 3.

### *3.4. The effect of MWCNT doping on the thermal stability of RCF-$Bi_2Te_3$ and RCF-$Bi_2S_3$ composites*

The TGA measurements for RCF-$Bi_2Te_3$ (0 wt% MWCNT) and

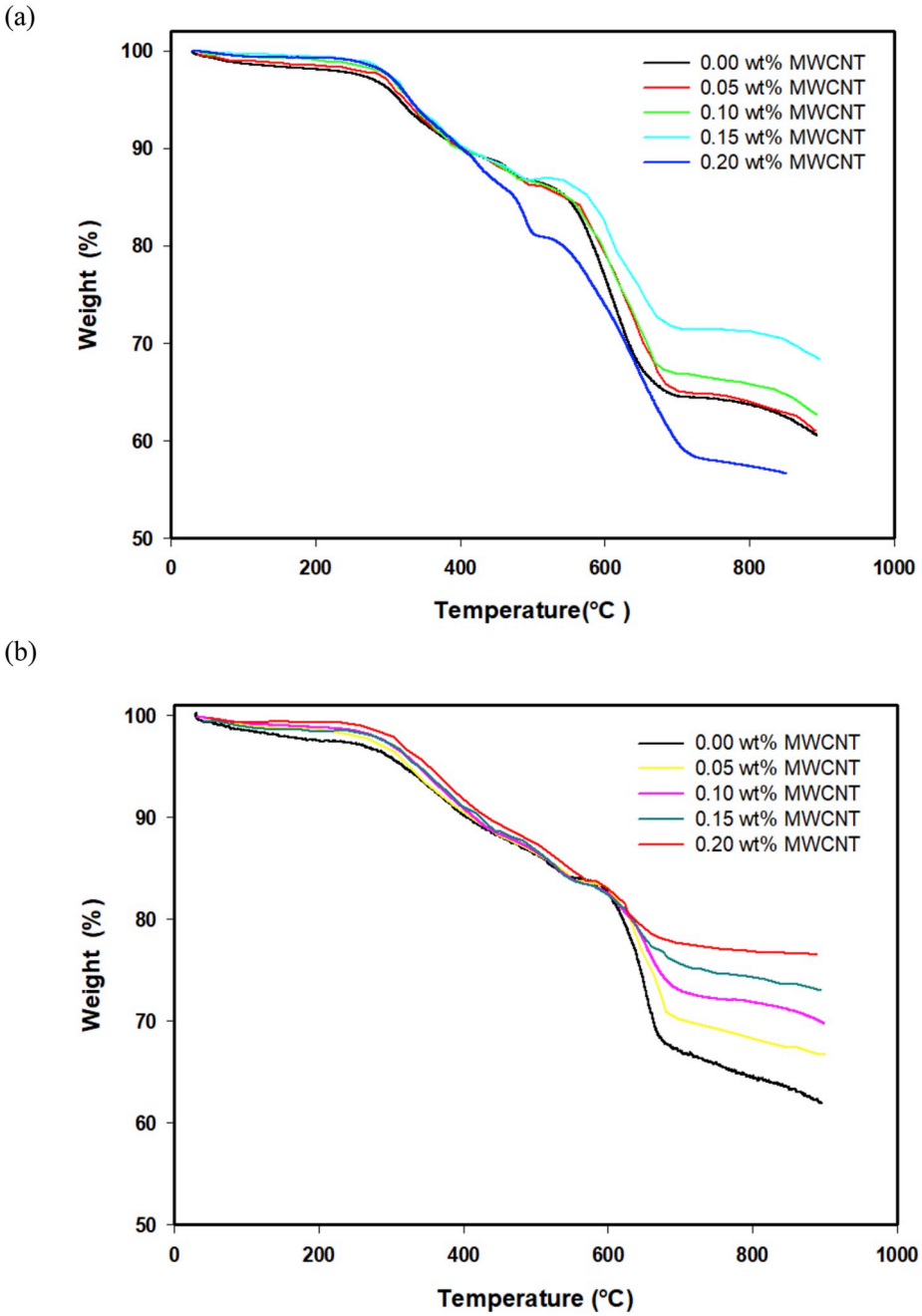


**Fig. 11.** TGA curves of (a) RCF-$Bi_2Te_3$ composites doped with various loadings of MWCNTs (b) RCF-$Bi_2S_3$ composites doped with various loadings of MWCNTs.

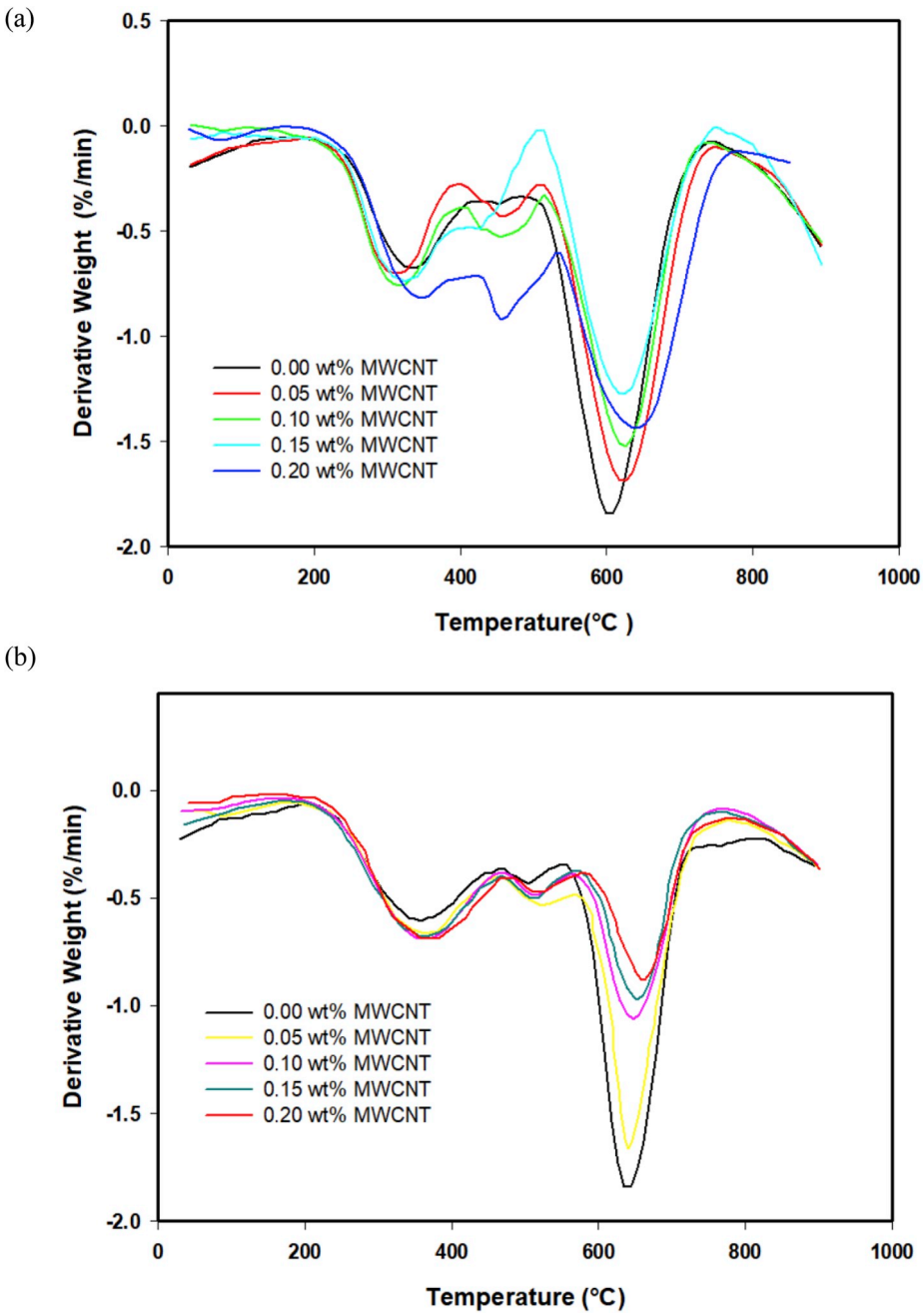


**Fig. 12.** DTG curves of (a) RCF-$Bi_2Te_3$ composites doped with various loadings of MWCNTs (b) RCF-$Bi_2S_3$ composites doped with various loadings of MWCNTs.

MWCNT doped RCF-$Bi_2Te_3$ composites with 0.05–0.20 wt% MWCNTs are shown in Fig. 11 (a). Based on Fig. 11 (a), MWCNTs improved the onset degradation temperature ($T_{onset}$) at 5% weight loss of RCF-$Bi_2Te_3$ composites from 316.2 °C (0 wt% MWCNT) to 330.75 °C (0.20 wt% MWCNT). The weight loss of composites decreased with increasing incorporation of MWCNT until 0.15 wt%. However, at higher concentration of 0.20 wt% of MWCNT the weight loss was seen to suddenly increase perhaps owing to the agglomeration of MWCNTs in the composite as explained in Section 3.2. Nevertheless, it can be concluded that doping of MWCNTs improved the thermal stability of RCF-$Bi_2Te_3$ composites if it is uniformly dispersed within the matrix. A similar improvement in weight loss and thermal stability of the composites were also observed in electrically conductive polymers doped with MWCNTs [47,49,51].

An improved onset degradation temperature ($T_{onset}$) at 5% weight loss was also observed for RCF-$Bi_2S_3$ composites doped with MWCNTs as shown in Fig. 11 (b). The TGA curves for MWCNT doped RCF-$Bi_2S_3$ composites were similar to those of RCF-$Bi_2S_3$. The $T_{onset}$ at 5% mass loss improved from 316.32 (0.00 wt% MWCNT) to 350.67 °C (0.20 wt% MWCNT).

The improvement in thermal stability of MWCNT doped RCF-$Bi_2Te_3$ composite is also highlighted in the improvement of the maximum degradation temperature ($T_{max}$) of the composites upon incorporation of MWCNT as shown in Fig. 12 (a). All the DTG curves upon incorporation of MWCNT shifted to the right showing an increase in the $T_{max}$ from 602.19 °C (0.00 wt% MWCNT) to 643.91 °C (0.20 wt% MWCNT). MWCNT doped RCF-$Bi_2S_3$ composite also showed a similar improvement in its $T_{max}$ as shown in Fig. 12 (b). The $T_{max}$ improved from 638.88 °C (0.00 wt% MWCNT) to 660.45 °C (0.20 wt% MWCNT) indicating that MWCNT has brought an improvement in its thermal stability.

When MWCNT is uniformly dispersed within the matrix, it is seen to improve the thermal stability (i.e. $T_{onset}$ and $T_{max}$) of both RCF-$Bi_2Te_3$

and RCF-$Bi_2S_3$ composites due to remarkable thermal properties of MWCNT [52]. Thermoelectric composites are constantly subjected to temperature variation cycles, thus it is imperative to have a thermoelectric composite that has robust thermal stability. MWCNT as a dopant is proven to be valuable in improving the thermal stability of RCF composites.

## 4. Conclusion

In summary, the optimum doping level of MWCNT for RCF-$Bi_2Te_3$ and RCF-$Bi_2S_3$ is 0.10 wt% and 0.15 wt% of MWCNTs, respectively. At optimum doping, MWCNT doped RCF-$Bi_2Te_3$ and RCF-$Bi_2S_3$ obtained power factors of 1.044 and 0.849 $\mu W K^{-2}m^{-1}$, respectively. At optimum doping level, MWCNTs enhanced the power factors of RCF-$Bi_2Te_3$ and RCF-$Bi_2S_3$ composites by approximately 438 and 800%, respectively. With the addition of MWCNT, the difference in power factor between RCF-$Bi_2Te_3$ and RCF-$Bi_2S_3$ was approximately 19%, whereas the difference in power factor without the addition of MWCNT between RCF-$Bi_2Te_3$ and RCF-$Bi_2S_3$ was approximately 52%. This is a validation of the capability of MWCNT to improve the power factor of the environmentally friendly $Bi_2S_3$ thermoelectric composites to a comparable value with that of $Bi_2Te_3$. At optimum doping levels, MWCNT also improved the crystallinity and thermal stability of the RCF-$Bi_2Te_3$ and RCF-$Bi_2S_3$ composites.

## Acknowledgement

The authors would like to thank the Ministry of Education Malaysia for PhD sponsorship under the MyBrain15 scholarship scheme.

## References

[1] Aswal DK, Basu R, Singh A. Key issues in development of thermoelectric power generators: high figure-of-merit materials and their highly conducting interfaces with metallic interconnects. Energy Convers Manag 2016;114:50–67.
[2] Zevenhoven R, Beyene A. The relative contribution of waste heat from power plants to global warming. Energy 2011;36:3754–62.
[3] Miner A. The industrialization of thermoelectric power generation technology. Maryland, Baltimore. 2012.
[4] Chen WH, Huang SR, Lin YL. Performance analysis and optimum operation of a thermoelectric generator by Taguchi method. Appl Energy 2015;158:44–54.
[5] Barma MC, Riaz M, Saidur R, Long BD. Estimation of thermoelectric power generation by recovering waste heat from Biomass fired thermal oil heater. Energy Convers Manag 2015;98:303–13.
[6] Champier D. Thermoelectric generators: a review of applications. Energy Convers Manag 2017;140:167–81.
[7] Yu YQ, Zhang BP, Ge ZH, Shang PP, Chen YX. Thermoelectric properties of Ag-doped bismuth sulfide polycrystals prepared by mechanical alloying and spark plasma sintering. Mater Chem Phys 2011;131:216–22.
[8] Ge Z-H, Qin P, He D, Chong X, Feng D, Ji Y-H, et al. Highly enhanced thermoelectric properties of Bi/Bi $_2$ S $_3$ nanocomposites. ACS Appl Mater Interfaces 2017;9:4828–34.
[9] Yoo BY, Huang C-K, Lim JR, Herman J, Ryan M a, Fleurial J-P, et al. Electrochemically deposited thermoelectric n-type Bi2Te3 thin films. Electrochim Acta 2005;50:4371–7.
[10] Wang X, He H, Wang N, Miao L. Effects of annealing temperature on thermoelectric properties of Bi 2 Te 3 films prepared by co-sputtering. Appl Surf Sci 2013;276:539–42.
[11] Pan Y, Wei TR, Cao Q, Li JF. Mechanically enhanced p- and n-type Bi2Te3-based thermoelectric materials reprocessed from commercial ingots by ball milling and spark plasma sintering. Mater Sci Eng B Solid-State Mater Adv Technol 2015;197:75–81.
[12] Du X, Cai F, Wang X. Enhanced thermoelectric performance of chloride doped bismuth sulfide prepared by mechanical alloying and spark plasma sintering. J Alloy Comp 2014;587:6–9.
[13] Biswas K, Zhao LD, Kanatzidis MG. Tellurium-free thermoelectric: the anisotropic n -type semiconductor Bi 2S 3. Adv Energy Mater 2012;2:634–8.
[14] Kunadian I, Andrews R, Pinar Mengüç M, Qian D. Thermoelectric power generation using doped MWCNTs. Carbon N Y 2009;47:589–601.
[15] Narducci D, Selezneva E, Cerofolini G, Frabboni S, Ottaviani G. Impact of energy filtering and carrier localization on the thermoelectric properties of granular semiconductors. J Solid State Chem 2012;193:19–25.
[16] Zou H, Rowe DM, Min G. Growth of p- and n-type bismuth telluride thin films, vol. 222; 2001. p. 82–7.
[17] Ma R, Liu G, Li J, Li Y, Chen K, Han Y, et al. Effect of secondary phases on thermoelectric properties of Cu2SnSe3. Ceram Int 2017;43:7002–10.
[18] Witik RA, Teuscher R, Michaud V, Ludwig C, Månson JAE. Carbon fibre reinforced composite waste: an environmental assessment of recycling, energy recovery and landfilling. Compos Part A Appl Sci Manuf 2013;49:89–99.
[19] Pimenta S, Pinho ST. Recycling carbon fibre reinforced polymers for structural applications: technology review and market outlook. Waste Manag 2011;31:378–92.
[20] Jagadish PR, Li LP, Chan A, Khalid M. Effect of annealing on virgin and recycled carbon fiber electrochemically deposited with N-type bismuth telluride and bismuth sulfide. Mater Manuf Process 2016;31.
[21] Jagadish PR, Khalid M, Amin N, Li LP, Chan A. Process optimisation for n-type Bi2Te3 films electrodeposited on flexible recycled carbon fibre using response surface methodology. J Mater Sci 2017;52.
[22] Jagadish PR, Khalid M, Li LP, Hajibeigy MT, Amin N, Walvekar R, et al. Cost effective thermoelectric composites from recycled carbon fibre: from waste to energy. J Clean Prod 2018:195.
[23] Wang D, Su Y, Chen D, Wang L, Xiang X, Zhu D. Preparation and characterization of poly(3-octylthiophene)/carbon fiber thermoelectric composite materials. Compos B Eng 2015;69:467–71.
[24] Kim M, Sung DH, Kong K, Kim N, Kim BJ, Park HW, et al. Characterization of resistive heating and thermoelectric behavior of discontinuous carbon fiber-epoxy composites. Compos B Eng 2016;90:37–44.
[25] Sung DH, Kang GH, Kong K, Kim M, Park HW, Park Y Bin. Characterization of thermoelectric properties of multifunctional multiscale composites and fiber-reinforced composites for thermal energy harvesting. Compos B Eng 2016;92:202–9.
[26] Yang W, Wang H, Liu T, Gao L. A Bi2S3@CNT nanocomposite as anode material for sodium ion batteries. Mater Lett 2016;167:102–5.
[27] Zhao Y, Liu T, Xia H, Zhang L, Jiang J, Shen M, et al. Branch-structured Bi 2 S 3 –CNT hybrids with improved lithium storage capability. J Mater Chem 2014;2:13854–8.
[28] Ni J, Zhao Y, Liu T, Zheng H, Gao L, Yan C, et al. Strongly coupled Bi2S3@CNT hybrids for robust lithium storage. Adv Energy Mater 2014;4:1–5.
[29] Memon AA, Patil SA, Sun KC, Mengal N, Arbab AA, Sahito IA, et al. Carbonous metallic framework of multi-walled carbon Nanotubes/Bi 2 S 3 nanorods as heterostructure composite films for efficient quasi-solid state DSSCs. Electrochim Acta 2018;283:997–1005.
[30] Ali A, Khan A, Ali A, Ahmad M. Pressure-sensitive properties of carbon nanotubes/bismuth sulfide composite materials. Nanomater Nanotechnol 2017;7:1–9.
[31] Zhao L, Sun X, Lei Z, Zhao J, Wu J, Li Q, et al. Thermoelectric behavior of aerogels based on graphene and multi-walled carbon nanotube nanocomposites. Compos B Eng 2015;83:317–22.
[32] Kim KT, Eom YS, Son I. Fabrication process and thermoelectric properties of CNT/Bi 2 ( Se , Te ) 3 composites. J Nanomater 2015:202415. 1–6.
[33] Kim KT, Choi SY, Shin EH, Moon KS, Koo HY, Lee G-G, et al. The influence of CNTs on the thermoelectric properties of a CNT/Bi2Te3 composite. Carbon N Y 2013;52:541–9.
[34] Lognone Q, Gascoin F. On the effect of carbon nanotubes on the thermoelectric properties of n-Bi2Te2.4Se0.6 made by mechanical alloying. J Alloy Comp 2015;635:107–11.
[35] Kim MY, Oh TS. Electrodeposition and thermoelectric characteristics of Bi 2Te 3 and Sb 2Te 3 films for thermopile sensor applications. J Electron Mater 2009;38:1176–81.
[36] Hasan BA, Shallal IH. Structural and optical properties of SnS thin films. J Nanotechnol Adv Mater 2014;2:43–9.
[37] Yücel E, Yücel Y. Fabrication and characterization of Sr-doped PbS thin films grown by CBD. Ceram Int 2017;43:407–13.
[38] Yücel E, Yücel Y. Effect of doping concentration on the structural, morphological and optical properties of Ca-doped PbS thin films grown by CBD. Opt - Int J Light Electron Opt 2017;142:82–9.
[39] Kumar S, Chaudhary D, Kumar Dhawan P, Yadav RR, Khare N. Bi2Te3-MWCNT nanocomposite: an efficient thermoelectric material. Ceram Int 2017;43:14976–82.
[40] Ebbesen TW, Lezec HJ, Hiura H, Bennett JW, Ghaemi HF, Thio T. Electrical conductivity of individual carbon nanotubes. Nature 1996;382:54.
[41] Zhang Y, Wang XL, Yeoh WK, Zheng RK, Zhang C. Electrical and thermoelectric properties of single-wall carbon nanotube doped Bi2Te3. Appl Phys Lett 2012;101:031909.
[42] Yu C, Kim YS, Kim D, Grunlan JC. Thermoelectric behavior of segregated-network polymer nanocomposites. Nano Lett 2008;8:4428–32.
[43] Bark H, Kim J-S, Kim H, Yim J-H, Lee H. Effect of multiwalled carbon nanotubes on the thermoelectric properties of a bismuth telluride matrix. Curr Appl Phys 2013;13:S111–4.
[44] Moriarty GP, Wheeler JN, Yu C, Grunlan JC. Increasing the thermoelectric power factor of polymer composites using a semiconducting stabilizer for carbon nanotubes. Carbon N Y 2012;50:885–95.
[45] Numan A, Shahid MM, Omar FS, Rafique S, Bashir S, Ramesh K, et al. Binary nanocomposite based on Co3O4 nanocubes and multiwalled carbon nanotubes as an ultrasensitive platform for amperometric determination of dopamine. Microchim Acta 2017;184:2739–48.
[46] Aghelinejad M, Leung SN. Fabrication of open-cell thermoelectric polymer nanocomposites by template-assisted multi-walled carbon nanotubes coating. Compos B Eng 2018;145:100–7.
[47] Du Y, Shen SZ, Yang W, Donelson R, Cai K, Casey PS. Simultaneous increase in conductivity and Seebeck coefficient in a polyaniline/graphene nanosheets thermoelectric nanocomposite. Synth Met 2012;161:2688–92.
[48] Xu H, Wang W. Electrodeposition of MWNT/Bi2Te3 composite thermoelectric films. J Electron Mater 2013;42:1936–45.

[49] Wang L, Jia X, Wang D, Zhu G, Li J. Preparation and thermoelectric properties of polythiophene/multiwalled carbon nanotube composites. Synth Met 2013;181:79–85.
[50] Manohari AG, Dhanapandian S, Manoharan C, Kumar KS, Mahalingam T. Effect of doping concentration on the properties of bismuth doped tin sulfide thin films prepared by spray pyrolysis. Mater Sci Semicond Process 2014;17:138–42.
[51] Wang J, Cai K, Shen S, Yin J. Preparation and thermoelectric properties of multi-walled carbon nanotubes/polypyrrole composites. Synth Met 2014;195:132–6.
[52] Chen G-X, Kim H-S, Park BH, Yoon J-S. Multi-walled carbon nanotubes reinforced nylon 6 composites. Polymer 2006;47:4760–7.